Ancilla-Assisted Quantum Process Tomography

J. B. Altepeter, D. Branning, E. Jeffrey, T. C. Wei, and P. G. Kwiat*

Department of Physics, University of Illinois at Urbana-Champaign, Urbana Illinois 61801-3080, USA

R. T. Thew,[†] J. L. O'Brien, M. A. Nielsen, and A. G. White[‡]

*Center for Quantum Computer Technology and School of Physical Sciences, University of Queensland, QLD 4072,
Brisbane, Australia*

Complete and precise characterization of a quantum dynamical process can be achieved via the method of quantum process tomography. Using a source of correlated photons, we have implemented several methods, each investigating a wide range of processes, e.g., unitary, decohering, and polarizing. One of these methods, ancilla-assisted process tomography (AAPT), makes use of an additional "ancilla system," and we have theoretically determined the conditions when AAPT is possible. Surprisingly, entanglement is *not* required. We present data obtained using both separable and entangled input states. The use of entanglement yields superior results, however.

Quantum information science [1] exploits quantum mechanics to achieve information processing tasks impossible in the classical world. Recent experiments [2] have reported the implementation of a wide variety of simple quantum information processing tasks. It is important to benchmark the performance of experimental systems as quantum information processing devices: one promising method, proposed in 1997, is *quantum process tomography* (QPT) [3]. Standard QPT (SQPT) involves preparing an ensemble of a number of *different* quantum states, subjecting each of them to the (fixed) quantum process to be characterized, and performing quantum state tomography on the outputs. An alternative to SQPT, which we refer to as *ancilla-assisted process tomography* (AAPT), introduces an extra *ancilla* qubit, and involves preparation and tomography of only a *single* two-qubit quantum state, rather than four one-qubit states [4]. As a special case, entanglement-assisted process tomography (EAPT) describes the situation when the ancilla is initially maximally entangled with the system being characterized.

To date, SQPT has been realized in liquid nuclear magnetic resonance systems [5] while SQPT and EAPT have been demonstrated in optical systems, but only for unitary transforms [6]. Here we describe optical implementations of SQPT, EAPT, and nonentangled AAPT for a variety of processes, including unitary, decohering, and non–trace-preserving (e.g., partial polarizing) operations. We also report a theoretical result completely characterizing the class of states usable for AAPT. An equivalent result was independently developed, and was reported just prior to our own [7].

In SQPT, a quantum system, *A*, experiences an unknown quantum process, $\mathcal{E}$. To determine $\mathcal{E}$ we first choose some fixed set of states $\{\rho_j\}$ which form a basis for the set of operators acting on the state space of system *A*, e.g., $\{\rho_j\} = \{\rho_H, \rho_V, \rho_D, \rho_R\}$ for a polarization

qubit (throughout this paper *H*, *V*, *D*, *A*, *R*, and *L* denote horizontal, vertical, diagonal, antidiagonal, right-circular, and left-circular polarization, respectively). Each state ρ_j is then subject to the process $\mathcal{E}$, and quantum state tomography [8–10] is used to experimentally determine the output $\mathcal{E}(\rho_j)$. $\mathcal{E}$ is fully characterized if we determine matrices E_j, known as *operation elements*, such that $\mathcal{E}(\rho) = \sum_j E_j \rho E_j^\dagger, \forall \rho$. This representation is known as an operator-sum decomposition [1].

In AAPT the process $\mathcal{E}$ is characterized by preparing a *single state*, σ, and then measuring $(\mathcal{E} \otimes I)(\sigma)$. This requires an *ancilla system*, *B*, with Hilbert space dimension at least as great as that of *A*. For an appropriate initial state, it is possible to characterize $\mathcal{E}$ by preparing the state σ, performing the process $\mathcal{E}$ on system *A*—leaving system *B* completely isolated—and taking a tomography of the output $(\mathcal{E} \otimes I)(\sigma)$. The total number of measurements is the same in AAPT (16 measurements on a single 2-qubit state) as in SQPT (four measurements on each of four input states).

AAPT has advantages over SQPT, most notably being that preparation of only a single quantum state is necessary for its operation. Consider the possibility of using it as a diagnostic tool in a quantum computer. When an unknown effect acts on less than half of a system of qubits, knowledge of the larger state before and after the change is sufficient to exactly predict the effect this change will have on every other state. (Assuming that the larger state is usable for AAPT—see below). Alternatively, SQPT has the advantage that it is generally easier to produce and measure states with fewer qubits.

We have investigated a variety of dynamical processes, using the three methods of SQPT, EAPT, and nonentangled AAPT. Our processes operate on the polarization state of a single photon. We used spontaneous parametric down-conversion (of a 351-nm pump beam) in a nonlinear crystal (BBO) to create pairs of time-correlated

photons at 702 nm. For SQPT, by triggering on one photon, the other was prepared into a single-photon state [11] with H polarization (Fig. 1). Half and quarter wave plates converted the horizontal polarization into an arbitrary state, thus allowing us to prepare the necessary input states ρ_H, ρ_V, ρ_D, and ρ_R. The tomography of the post-process states was performed by measuring (in coincidence with the trigger detector) the Stokes parameters $S_1 = P_H - P_V$, $S_2 = P_D - P_A$, and $S_3 = P_R - P_L$, and performing a maximum-likelihood estimation of the density matrix [9]. (Here P_i denotes a *probability*: calculated as the intensity of a state measured in the ith basis divided by the total intensity.) Typical measurements yielded a maximum of 13 000 photon counts over 30 sec.

For our EAPT results, two adjacent BBO crystals were used to prepare the maximally entangled state $|\phi^-\rangle = (|HH\rangle - |VV\rangle)/\sqrt{2}$ [12]. One of the resulting qubits was subjected to the given process, and two-qubit tomography of the pair was then performed by measuring the polarization correlations of the photons with 16 measurements, e.g., in the following bases: HH, HV, HD, HR, VH, VV, etc. [8]. Note from Fig. 1 that the elements used in SQPT to prepare the single-photon state are now placed (in reverse order) in the other detection arm, highlighting the symmetry of the two techniques.

We also performed AAPT using the nonentangled Werner state $\rho_W = \frac{1}{6}I + \frac{1}{3}|\gamma\rangle\langle\gamma|$, where $|\gamma\rangle$ is a maximally entangled state. To prepare this state we adjust the polarization of the pump beam until the down conversion crystals produce the pure, partially entangled state

$[1/\sqrt{6}(\sqrt{2}-1)]|HH\rangle + [(\sqrt{2}-1)/\sqrt{6}]|VV\rangle$ [8]. A half wave plate at 22.5° in each arm then transforms this state into $|\phi\rangle = \sqrt{1/3}|HH\rangle + \sqrt{1/6}|HV\rangle + \sqrt{1/6}|VH\rangle + \sqrt{1/3}|VV\rangle$. Next we pass each photon through a decoherer, an 11-mm piece of quartz which separates the H and V components of the polarization by $\sim100\ \mu$m, which is the coherence length of the individual photons [determined by the 3-mm diam collection irises and the 5-nm bandwidth (FWHM) interference filters]. This destroys all coherence terms in $|\phi\rangle\langle\phi|$ except for $|HH\rangle\langle VV|$ and $|VV\rangle\langle HH|$. An additional, shorter decoherer in the idler arm lowers these terms to achieve a state which has $99.2 \pm 0.8\%$ fidelity [13] with the above Werner state.

For single-qubit processes, a convenient graphical representation plots the transformation of the sphere of all possible states (e.g., the Poincaré sphere for polarization) [1], as determined by the action of the process on the set of basis states, ρ_j. For example, all unitary transformations are equivalent to a rotation about some axis [Fig. 2(b)]. Decoherence is represented by a collapsing of the sphere toward a "spindle" [Fig. 2(c)]; for instance, complete decoherence in the HV basis leaves the states $|H\rangle$ and $|V\rangle$ unmodified, but transforms the states $|D\rangle$ and $|R\rangle$ into the completely mixed state at the center of the
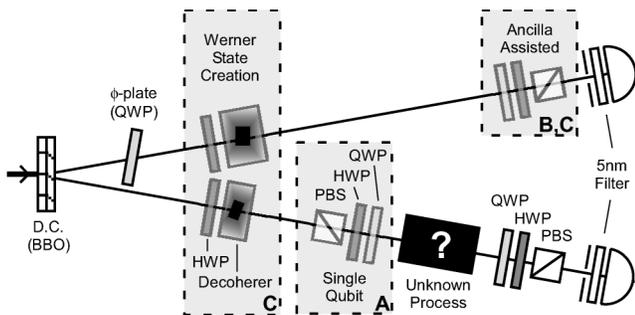

FIG. 1. Experimental arrangements to perform quantum process tomography. A 351-nm pump is directed through two 0.6 mm-thick BBO crystals, giving rise to pairs of correlated photons at 702 nm, detected using Si avalanche photodiodes and fast coincidence electronics. A, B, and C above denote which elements are present for SQPT, EAPT, and nonentangled AAPT, respectively. (a) SQPT: Polarizer (P), half-wave plate (HWP) and quarter-wave plate (QWP) allow preparation of required pure single photon (conditioned on "trigger" detection) states; identical elements allow tomography of the post-process states. (b) EAPT: The source produces the maximally entangled state $(|HH\rangle - |VV\rangle)/\sqrt{2}$. A two-photon tomography of the output allows reconstruction of the process. (c) AAPT: The source produces $\rho_W \sim \frac{1}{6}I + \frac{1}{3}|\gamma\rangle\langle\gamma|$, where $|\gamma\rangle$ is a maximally entangled state. Although there is no entanglement, the correlations in ρ_W allow AAPT.
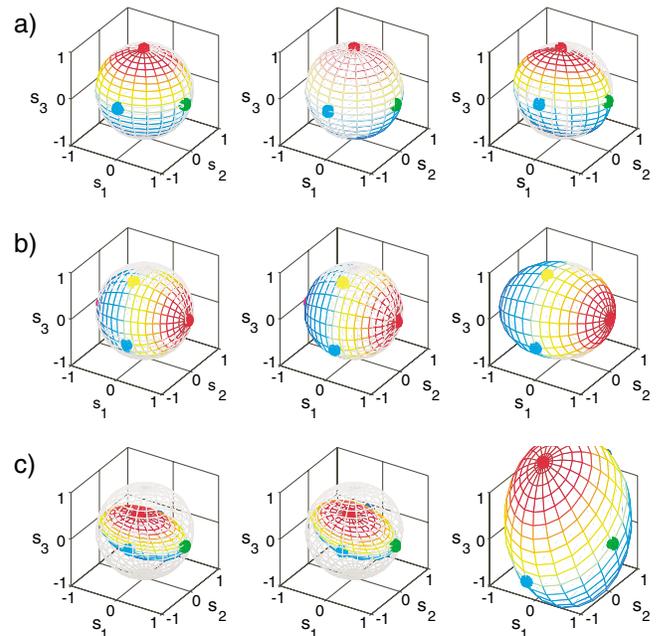

FIG. 2 (color). Geometric mappings for three quantum processes—(a) identity, (b) unitary transformation, and (c) decoherence—measured using SQPT (left), EAPT (center), and AAPT (right). The axes are the Stokes parameters (S_1, S_2, S_3). The colored mesh surfaces show how all pure states are transformed by the process. The initial states H, R, V, and A are shown by the green, red, yellow, and blue dots, respectively. The transformation of initial *mixed* states (inside the surface) may be interpolated from the pure state results using the linearity of quantum mechanics. The mesh coloring denotes the orientation of the transformed sphere.

sphere. This graphical approach can even be applied to lossy processes, e.g., partial polarizers, though it is important to note that it does not indicate the amount of loss, only the quantum state of the surviving qubits.

We now outline the general procedure for SQPT, as described in [3]. Rather than directly determining the operation elements E_j, SQPT relates these to a fixed set of operators, $\{\tilde{E}_m\}$, where $E_j = \sum_m e_{jm}\tilde{E}_m$ and e_{jm} can be complex. This allows us to define a *single* matrix, χ, that fully characterizes the process: if we rewrite the process as $\mathcal{E}(\rho) = \sum_{mn} \tilde{E}_m \rho \tilde{E}_n^\dagger \chi_{mn}$ then χ is a positive Hermitian matrix, $\chi_{mn} = \sum_k e_{km} e_{kn}^*$. See Fig. 3 for examples of experimentally determined χ matrices. To determine χ, we choose a set of basis states $\{\rho_j\}$, such that for each input state ρ_j, state tomography returns an output, $\mathcal{E}(\rho_j) = \sum_k c_{jk}\rho_k$. If we define $\tilde{E}_m \rho_j \tilde{E}_n^\dagger = \sum_k \beta_{jk}^{mn}\rho_k$ (where β_{jk}^{mn} is another complex number matrix which we determine from our choice of input basis states $\{\rho_j\}$, output basis states $\{\rho_k\}$, and operators $\{\tilde{E}_j\}$), we can see that $\sum_k \sum_{mn} \chi_{mn} \beta_{jk}^{mn}\rho_k = \sum_k c_{jk}\rho_k$, independent of ρ_k; β is invertible; and $\chi_{mn} = \sum_{jk}(\beta^{-1})_{jk}^{mn} c_{jk}$.

In our experiment we use $\{\tilde{E}_m\} = \{I, \sigma_x, \sigma_y, \sigma_z\}$, respectively equivalent to the following optical elements: nothing; a half-wave plate (HWP) at 45°; an optically active element; a HWP plate at 0°. The diagonal elements of the χ-matrix correspond, respectively, to the probability of carrying out the I, σ_x, σ_y, and σ_z processes, while the off-diagonal elements correspond to *coherence* processes of the form $\sigma_x \rho \sigma_y$ and $\sigma_y \rho \sigma_x$, etc.

We investigated several processes, including the identity, a unitary rotation, a decoherer, and both a coherent and an incoherent partial polarizer (see below). The results for the identity process measure how well the input state(s) are preserved. We used SQPT, EAPT, and AAPT to measure the same unitary rotation process (a birefringent wave plate). The results were in close agreement [Fig. 2(b)]; the resulting χ matrices had an average process fidelity [14] between the three methods of $\mathcal{F} = (100.4 \pm 0.8)\%$. Likewise, the SQPT and EAPT measurements of a decohering process (implemented with a 6.3-mm piece of quartz) yielded $\mathcal{F} = (99.9 \pm 0.3)\%$ [Fig. 2(c)]. The same process, when measured using our Werner state, appears to be a *recoherer*—a process which is not a positive map. This Werner state was prepared using a thick piece of quartz to temporally separate the H and V components of the light, introducing decoherence.
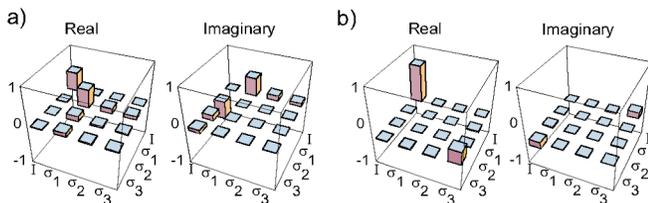
Consider adding another piece of quartz, with optic axis perpendicular to the first, after the original. This also temporally shifts the H and V components of the light, but in the opposite direction, undoing the original decoherence. Our decohering process does exactly this, effectively *recohering* the Werner state—impossible for a 1-qubit process. The resolution to this paradox lies in the assumption that the measured process does not act on any degrees of freedom used to prepare the input state other than the tested qubit. For example, if frequency is traced over to prepare a mixed input state, a process that couples to frequency cannot be measured.

Coherent and incoherent partial polarizers were measured in order to highlight the role coherence plays in lossy processes. A glass plate at Brewster's angle to an incident beam is a coherent partial polarizer, as the operation of the plate maintains the preexisting phase relationship between the horizontal component of the light (completely transmitted) and the vertical component of the light (partially reflected). For the incoherent case, consider inserting a horizontal polarizer into the beam 50% of the time. Half the time only the horizontal component of the light will be transmitted, but more importantly, the transmitted light will have no coherence relationship with the light that does not pass through the polarizer. For the coherent partial polarizer, pure states remain pure but slide toward H along the surface of the sphere. In the incoherent case pure states travel linearly through the sphere to H, becoming mixed (Fig. 4).

What class of initial states σ of the AB system may be used for AAPT? This question can be answered using an
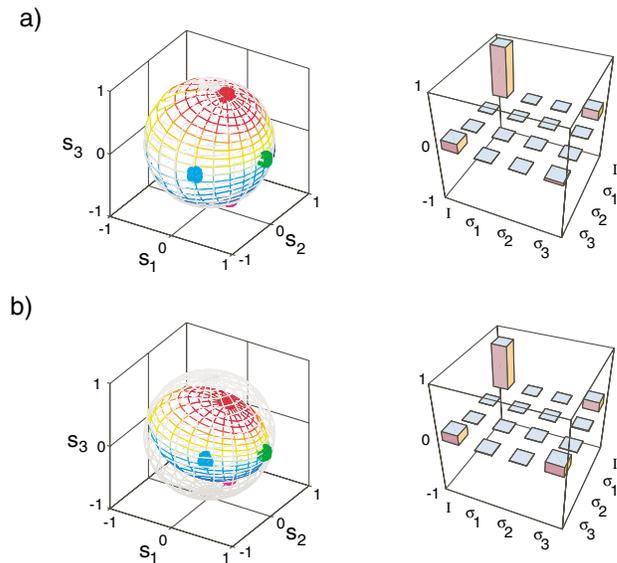
FIG. 4 (color). Geometric mappings and χ matrices for (a) coherent and (b) incoherent partially polarizing processes. The former was implemented using two glass microscope slides near Brewster's angle [$T_H \sim 88\%, T_V \sim 45\%$]. The latter was simulated by inserting a horizontal polarizer 50% of the time. (Real components shown; imaginary contributions $<1\%$.)

FIG. 3 (color online). χ matrices determined from EAPT for (a) unitary and (b) decohering processes, as shown in Fig. 2.

operator generalization of the Schmidt decomposition for entangled states [1]. First, we introduce an inner product on operators, $(M, N) \equiv \mathrm{tr}(M^\dagger N)$, and define an orthonormal operator basis to be a set of operators $\{M_j\}$ such that $(M_j, M_k) = \mathrm{tr}(M_j^\dagger M_k) = \delta_{jk}$. (For example, an orthonormal basis for single-qubit operators is the set $\{I/\sqrt{2}, \sigma_x/\sqrt{2}, \sigma_y/\sqrt{2}, \sigma_z/\sqrt{2}\}$). The operator-Schmidt decomposition [15] states that an operator M acting on AB can be decomposed as $M = \sum_l s_l A_l \otimes B_l$, where the s_l are non-negative real numbers, and the sets $\{A_l\}$ and $\{B_l\}$ form orthonormal operator bases for systems A and B, respectively [16]. The *Schmidt number* $\mathrm{Sch}(M)$ of an operator M is defined [15] as the number of nonzero terms in the Schmidt decomposition.

A state σ of AB may be used to perform AAPT *if and only if* the Schmidt number of σ is d_A^2, where d_A is the dimension of the state space of system A. Consider that in order to measure the mapping of the entire space, the input state must possess correlations—represented by the Schmidt number—between enough states to form a basis for the mapping. To prove this, expand σ in its Schmidt decomposition as $\sigma = \sum_l s_l A_l \otimes B_l$. Assume σ has Schmidt number d_A^2, so that the A_l form an orthonormal operator basis, and $s_l > 0$ for all l. Let σ' be the output obtained after letting $\mathcal{E}$ act on system A, that is, $\sigma' = (\mathcal{E} \otimes I)(\sigma) = \sum_l s_l \mathcal{E}(A_l) \otimes B_l$. By the orthonormality of the B_l and the previous equation it follows that $\mathrm{tr}_B[(I \otimes B_m^\dagger)\sigma'] = \sum_l s_l \mathcal{E}(A_l)\mathrm{tr}(B_m^\dagger B_l) = s_m \mathcal{E}(A_m)$, and so $\mathcal{E}(A_m) = \mathrm{tr}_B[(I \otimes B_m^\dagger)\sigma']/s_m$. The fact that the Schmidt number of σ is d_A^2 ensures that $s_m > 0$, so there is no problem with division by zero. By doing state tomography on σ' and applying the above equation, it is possible to determine the action of $\mathcal{E}$. The techniques described earlier can then be used to generate a χ matrix or transformed sphere.

Conversely, let E_A be the space of trace-preserving quantum operations on system A, and let S_{AB} be the space of quantum states on system AB. Define a map $f : E_A \to S_{AB}$ by $f(\mathcal{E}) \equiv (\mathcal{E} \otimes I)(\sigma)$. For AAPT, we require that f be a one-to-one map, i.e., there are never two distinct operations such that $f(\mathcal{E}_1) = f(\mathcal{E}_2)$. A parameter counting argument shows that f cannot be one-to-one when σ has Schmidt number less than d_A^2. The dimensionality of the manifold E_A is $d_A^4 - d_A^2$. Since $f(\mathcal{E}) = \sum_l s_l \mathcal{E}(A_l) \otimes B_l$, the dimension of the image manifold $f(E_A)$ is at most $\mathrm{Sch}(M) \times (d_A^2 - 1)$, because the map $\mathcal{E} \to \mathcal{E}(A_l)$ has image of dimension at most $d_A^2 - 1$. Thus, for AAPT we require that $\mathrm{Sch}(M) \times (d_A^2 - 1) \geq d_A^4 - d_A^2$, which is only possible when $\mathrm{Sch}(M) = d_A^2$.

Note that AAPT is possible only when the dimension of system B is at least as great as the dimension of system A. When this is true, almost all states of system AB may be used for AAPT, because the set of states with Schmidt number less than d_A^2 has measure zero. That is, a maximally entangled input is not required for AAPT—indeed many of the viable input states are not entangled at all, as

demonstrated by our Werner state AAPT. However, while almost any state *can* be used for AAPT, maximally entangled states appear to be experimentally optimal in that they have perfect nonlocal correlations. Figure 2 highlights this difference, as the AAPT results have significantly greater statistical errors than the EAPT (both were from identical measurement runs). This comparative usefulness of entangled versus separable states was first introduced and is discussed further in [7].

---

*Electronic address: kwiat@uiuc.edu
†Group of Applied Physics, University of Geneva, 1211 Geneva 4, Switzerland.
‡Electronic address: andrew@physics.uq.edu.au

[1] M. A. Nielsen and I. L. Chuang, *Quantum Computation and Quantum Information* (Cambridge University Press, Cambridge, 2000).

[2] *Proceedings of the International Conference on the Experimental Implementation of Quantum Computation, Sydney, 2001*, edited by R. G. Clark (Rinton Press, Princeton, NJ, 2001).

[3] I. L. Chuang and M. A. Nielsen, J. Mod. Opt. **44**, 2455 (1997); J. F. Poyatos, J. I. Cirac, and P. Zoller, Phys. Rev. Lett. **78**, 390 (1997).

[4] D. Leung, Ph.D. thesis, Stanford University, comp-sci/0012017; G. M. D'Ariano and P. Lo Presti, Phys. Rev. Lett. **86**, 4195 (2001); W. Dür and J. I. Cirac, Phys. Rev. A **64**, 012317 (2001).

[5] M. A. Nielsen, E. Knill, and R. Laflamme, Nature (London) **396**, 52 (1998); A. M. Childs, I. L. Chuang, and D. W. Leung, Phys. Rev. A **64**, 012314 (2001).

[6] F. De Martini, G. D'Ariano, A. Mazzei, and M. Ricci, quant-ph/0207143; quant-ph/0210210; Y. Nambu *et al.*, Proc. SPIE Int. Soc. Opt. Eng. **4917**, 13 (2002).

[7] G. D'Ariano and P. Lo Presti, quant-ph/0211133. Private communications showed this work was in development as early as 2001.

[8] A. G. White, D. F. V. James, P. H. Eberhard, and P. G. Kwiat, Phys. Rev. Lett. **83**, 3103 (1999).

[9] D. F. V. James, P. G. Kwiat, W. J. Munro, and A. G. White, Phys. Rev. A **64**, 052312 (2001).

[10] R. T. Thew, K. Nemoto, A. G. White, and W. J. Munro, Phys. Rev. A **66**, 012303 (2002).

[11] C. K. Hong and L. Mandel, Phys. Rev. Lett. **56**, 58 (1988).

[12] P. G. Kwiat *et al.*, Phys. Rev. A, **60**, R773 (1999).

[13] $F(\rho_1, \rho_2) = (\mathrm{Tr}\sqrt{\sqrt{\rho_1}\rho_2\sqrt{\rho_1}})^2$, which—for ρ_1 or ρ_2 pure—simplifies to $\mathrm{Tr}(\rho_1\rho_2)$ [2].

[14] $\mathcal{F}(\mathcal{E}_1, \mathcal{E}_2) \equiv \int d\psi F[\mathcal{E}_1(|\psi\rangle\langle\psi|), \mathcal{E}_2(|\psi\rangle\langle\psi|)]$. This was calculated numerically for our reported results. See Bowdrey *et al.*, Phys. Lett. A **294**, 258 (2002).

[15] M. A. Nielsen, Ph.D. thesis, University of New Mexico, 1998, quant-ph/0011036.

[16] Proof: M. A. Nielsen *et al.*, quant-ph/0208077.